Interactions between Silica-coated Gold Nanorods Substrates and Hydrophobic Analytes in Colloidal Surface-enhanced Raman Spectroscopy

*Hyunho Kang and Christy Haynes**

Department of Chemistry, University of Minnesota, 207 Pleasant Street SE, Minneapolis, MN 55455, United States

*Corresponding author, chaynes@umn.edu

Abstract

Surface-enhanced Raman scattering (SERS)-based detection of suspension phase analytes holds great promise for a variety of applications; however, plasmonic colloidal SERS substrates are not stable in many solution conditions unless they are protected by a stabilizing shell. Mesoporous silica shells on plasmonic nanoparticle cores have been demonstrated to perform well in a variety of liquid matrices. However, this silica shell can be seen as barrier from the perspective of the analyte, as the analyte molecules need to reach the plasmonic core after they pass through the shell. In this work, mesoporous silica-coated gold nanorods have been synthesized and characterized as aqueous colloidal SERS substrates systematically considering how SERS performance is impacted by three different factors: adsorbed molecules, the silica shell, and bulk solvent media. The results show that SERS signal intensities from the model hydrophobic analyte, trans-1,2-bis(4-pyridyl) ethylene (BPE), is enhanced when the pore size, hydrophobicity of the shell, and ionic strength are increased, indicating more favorable interaction between the substrates and the analyte. The silica shell presented herein facilitates efficient adsorption of the analyte to the gold core and enhanced sensitivity to

environmental refractive index changes. This efficient adsorption can be further enhanced by controlling the incubation temperature. Overall, this work reveals how substrate exposure conditions can be tuned to maximize analyte SERS signals without compromising the silica shell that protects the plasmonic properties of the SERS-enhancing core.

Introduction

In recent years, researchers have exploited nanoscience to pioneer and develop various technologies in fields such as manufacturing materials, biomedicine, and optics.[1–4] The tremendous demand for advanced nanomaterials has prompted research into a variety of nanoparticle platforms; among the most investigated since the early 1990s is the core-shell nanoparticle.[5–7] The core-shell structure often enhances the functional properties of nanomaterials by modifying the constituent materials, morphologies, or the ratio of core to shell.[8] Often, this core-shell structure yields enhanced stability of the inner core material, conserving critical physical and chemical properties and expanding the potential applications of these nanoparticles into many fields.[9,10]

Surface-enhanced Raman scattering (SERS) spectroscopy, a detection method that shows great potential in chemical sensing, can benefit greatly from the core-shell nanoparticle structure. SERS was discovered when Van Duyne et al. recognized the enhanced Raman scattering signals of adsorbed pyridine molecules on roughened silver electrodes in 1977.[11] This discovery generated significant interest to understand the electromagnetic and chemical mechanisms of SERS enhancement and in the development of materials to maximize enhancement factors. Over 40 years of debate and

research have shown that far-field SERS enhancement is largely governed by the localized surface plasmon resonance (LSPR), the coherent oscillation of conduction band electrons at the surface of plasmonic nanostructures that generates electromagnetic fields; these fields enhance the induced dipole in molecules near the plasmonic structure, thus enhancing the Raman scattering signals.[12] The LSPR is strongly dependent on the nanostructures' material properties and morphologies.[13,14] Regardless of the plasmonic material chosen, from gold or silver to copper or palladium,[15] the molecule to be enhanced must dwell within a few nanometers of the nanostructure surface; this requirement leads to an obvious tension between having molecules near to or adsorbed at a nanostructure surface and the need for stable plasmonic nanostructures. As such, the stabilization of the plasmonic properties of metals has been a critical challenge for researchers to design effective SERS platforms. For example, in 2010 Tian and co-workers fabricated the shell-isolated nanoparticle-enhanced Raman spectroscopy (SHINERS) platform by coating gold nanoparticles with thin shells of alumina or silica.[16] Many researchers have expanded and diversified this SHINERS platform by synthesizing ultrathin shell-coated gold or silver nanoparticles with different materials such as silica, carbon, alumina, and manganese oxide.[17–20] Recently, iodide-coated silver and liposome-based, protein-coated gold nanoparticle substrates have also been developed as biocompatible SERS substrate platforms.[21,22]

For the purpose of stabilization and isolation of metal nanoparticle cores from the external environment, silica has much potential as a shell and has been studied in many laboratories with distinct synthetic approaches.[10] The biocompatibility of silica has been demonstrated; this highly condensed dielectric shell is generally much more robust than

other bio-friendly molecular coating materials such as chitosan or dextran.[23] Furthermore, to enhance colloidal stability and modify the chemical properties of the silica shell, different types of silanes, such as those with polyethylene glycol functionality, can easily be condensed onto the surface of the shell in one pot syntheses.[24] The particle size can be tuned and recent studies show the clear scalability to produce a large amount of particles from a synthetic standpoint.[25,26] Thus, for colloidal SERS, addition of a silica shell to promote maintenance of the plasmonic core shape and LSPR can be used to obtain stable and consistent SERS performance. Clearly, it is also critical that the silica shell present porosity so that the target analytes can reach the core surface. Several research groups have developed and studied mesoporous silica-coated AuNRs (AuNRs@$mSiO_2$) for various applications such as imaging, biosensing, and cancer theragnostic platforms.[27–29] In 2016, we investigated the ability of AuNRs@$mSiO_2$ as an in-solution SERS substrate.[30] In that initial work, cetyltrimethylammonium bromide (CTAB) micelle formation was used during the coating process to generate mesoporous structures within the silica shell. These mesopore structures afforded analyte access to the gold cores and acted as a physical cut-off filter, limiting the molecular size of analytes that could reach the plasmonic core.

Herein, we probe further into the chemical and physical characteristics that control access of hydrophobic analytes, in this case trans-1,2-bis(4-pyridyl)ethylene (BPE), to the substrate of AuNRs@$mSiO_2$ for aqueous colloidal SERS. The results demonstrate that the hydrophobicity of and pore size within the silica shell influence access of the analyte molecules to the enhancing core. The bulk solution environmental parameters, such as ionic strength and temperature were tuned to observe the diffusion and adsorption

behaviors of the analytes in varying conditions. Further, extreme solvent mixture conditions were prepared to see if the viscosity, which is related to the diffusion rate of the analytes and substrates, affects the time-dependent SERS signal magnitude significantly. Overall, this work demonstrates that the interaction between BPE and AuNRs@mSiO_2 can be affected by the physical and chemical state of the silica shells as well as bulk environmental conditions. Importantly, the silica shell of the substrate successfully maintained plasmonic properties of the gold cores in all conditions considered, allowing stable diffusion and adsorption of BPE and thus, strong Raman signals. Overall, this systematic investigation will benefit all those working to exploit suspension-phase SERS sensing of hydrophobic analytes as well as those using core-shell nanostructure-based sensors with other signal transduction mechanisms.

Materials and methods

Materials

CTAB-stabilized AuNRs (LSPR λ_{max} = 798 nm) were purchased from Nanohybrids. Tetraethylorthosilicate (TEOS, 98%), hexadecyltrimethylammonium bromide (CTAB, 98%), chlorotrimethylsilane (TMS, 98%), 1,2-di(4-pyridyl)ethylene (BPE, 97%), and glycerol were purchased from Sigma Aldrich. 2-[methoxy(polyethyleneoxy)$_{9-12}$propyl]trimethoxysilane (PEG, molecular weight 591-723 g/mol) was purchased from Gelest. All chemicals were used without further purification.

Synthesis of silica-coated gold nanorods

A modified Stöber method was used to synthesize mesoporous silica-coated gold

nanorods (AuNRs@$mSiO_2$).[31] Powdered CTAB and decane were added to water to yield concentrations of 1.0 mM CTAB and 1.5 mM of decane; the solution was then sonicated for one hour before further use. After sonication, the micelle suspension was formed and had a slightly blue hue. The suspension was then removed from the sonication bath and allowed to cool undisturbed at room temperature. Next, 10 mL of the as-purchased AuNR suspensions from Nanohybrids (1 mM CTAB-stabilized in water, OD = 1.1, 0.045 mg/mL of Au) was centrifuged at 8000 rcf for 30 min to lower the CTAB concentration. Any additional centrifugation resulted in destabilization and aggregation among the suspended AuNRs. The supernatant was removed, and the pellets were resuspended in 1 mL of the CTAB-decane micelle suspension to yield a concentration of 1 nM AuNRs. This suspension was transferred to 15 × 34 mm vials containing a magnetic stirring bar that stirred the suspension for at least 3 hours at room temperature. Then, 5 μL of 0.1 M NaOH was added to adjust the pH to >10.0, and the suspension was further stirred for 30 min. Next, 4 μL of 20% TEOS in ethanol was added, and the suspension was stirred again for 24 hours.

For non-surface-modified AuNRs@$mSiO_2$, the silica-coated nanorods were transferred to centrifuge tubes and centrifuged at 8000 rcf for 20 min. To remove the surfactant, the supernatant was removed, and the pellets were re-suspended in 6 mL of ethanolic ammonium nitrate solution (6 g of NH_4NO_3 in 1 L ethanol) and refluxed twice for 30 min at 60°C. After reflux, the suspension was washed three times via centrifugation in 99% ethanol. For TMS-modified AuNRs@$mSiO_2$, after 24 hours of hydrolysis and condensation of TEOS to form silica shells, 5 μL of 0.1 M NaOH was added again and

stirred for 30 min. 4 μL of TMS was then added to the suspension, and the suspension was stirred for 48 hours. The purification method was the same as described above, and the final products were stored in 99% ethanol until use.

Material Characterization

Transmission Electron Microscopy (TEM). TEM images were taken with FEI Tecnai T12 at 120 kV. The purified nanoparticles were dispersed in ethanol, and Formvar/carbon-coated copper grids (Ted Pella, INC, Redding, CA) were dipped into the ethanolic suspensions. The grids were then dried in air to prepare the TEM samples.

Dynamic Light Scattering (DLS) and ζ-Potential Measurements. A Brookhaven 90Plus particle analyzer (Holtsville, NY) equipped with a 35 mW red diode laser (660 nm) was used to measure the hydrodynamic diameters of the nanoparticles. The AuNRs@mSiO_2 nanoparticles were suspended in water at a AuNR concentration of 0.2 mg/mL. For each measurement, a one-minute run was performed three times and averaged. To eliminate any possible interference (e.g. from dust), the suspensions were filtered with 0.45 μm GHP filter before measuring. For the ζ-potential measurements, the same concentration of nanoparticles was used, and a Brookhaven ZetaPALS Zeta-Potential Analyzer (Holtsville, NY) was utilized for the measurement. Five runs, each consisting of ten cycles, were run for each measurement. In each case, the ten measured zeta potentials were averaged, and then the five runs were further averaged.

UV-Vis Spectroscopy measurement. UV-Vis extinction spectra were measured with DH-2000 light source (Oceans Optics, Largo, FL). For the measurement, 300 μL of pure water or varying concentration of aqueous BPE solution was added into disposable micro UV

cuvettes. Then, 20 μL of concentrated (15 mg/mL, AuNR concentration) CTAB-stabilized or AuNRs@$mSiO_2$ were added to the cuvettes and mixed well before UV-Vis spectra measurement.

SERS measurement

1,2-di(4-pyridyl)ethylene (BPE) was chosen as the model hydrophobic analyte for this work based on being well-characterized for SERS and similar in size to many small molecules that are important SERS targets (Figure S1). The BPE was dissolved in 10 mL of DI-water at a concentration of 100 ppm with sonication. The analyte solution was then filtered to remove any undissolved BPE and serially diluted to achieve different concentrations. Concentrated nanoparticle substrate suspensions were prepared by transferring AuNRs@$mSiO_2$ (or AuNRs@$mSiO_2$-TMS) in ethanol to water at a final concentration of 1.0 to 6.0 mg/mL of AuNRs. Next, 10 μL of this concentrated substrate suspension was transferred to centrifuge tubes containing 110 μL of the analyte solution. After a brief vortexing, 8 μL of the analyte-substrate mixture was transferred to a plastic chip well. The well contents remained inside the well due to capillary forces despite the chip being held upright for SERS measurement (Figure S2a). The Snowy Range Sierra spectrometer used in this work has a laser excitation wavelength of 785 nm, and the parameters used for the experiments were 9 mW power and 30 second integration times.

For incubation in high ionic strength solutions, BPE aqueous solutions of 200 mM sodium chloride, ammonium acetate, and lithium perchlorate were prepared along with BPE salt-free aqueous solution. After the concentrated substrate suspensions were added in the

same way described above, SERS spectra were measured immediately after mixing and then after 30 and 60 minutes of incubation at room temperature.

For SERS experiments with varying parameters, the basic procedure was the same with slight modifications. For each different type of experiment, the analyte-substrate mixtures were incubated under slightly different conditions to test the importance of each condition. For the experiment varying incubation temperatures, 4 aqueous mixtures of BPE and AuNRs@mSiO$_2$-TMS were prepared, and each solution was incubated at a different temperature for 10 minutes after the addition of the substrates. SERS spectra were measured every hour for each mixture.

For the SERS measurement with glycerol mixtures, two different experiments were performed. In the first experiment, 20 μL of concentrated AuNRs@mSiO$_2$ in glycerol (6.0 mg/mL) was added to the vial first. Then, 1 mL of aqueous 50 ppb BPE solution were added to the vial. Each vial of the same concentration of the substrate and the analyte was then incubated at different temperatures as described earlier with/without stirring for 10 minutes. In the second experiment, 50 ppb of BPE solution in different glycerol/water mixtures (no glycerol, 30, 50, 70, and 90% glycerol by volume%) were prepared first. Then, into 110 μL of each mixture, 10 μL of concentrated AuNRs@mSiO$_2$ (1.0 mg/mL) in water were added to each mixture, and SERS spectra were measured at different time points.

Results and Discussion

Synthesis of Colloidal SERS AuNRs@mSiO$_2$ Substrates

The synthetic scheme to make AuNRs@mSiO$_2$-TMS is described in Figure 1a. The as-purchased AuNRs arrived suspended in 1 mM CTAB, so the AuNRs were centrifuged once to lower the CTAB concentration. Any further centrifugation or use of the centrifuge at higher relative centrifugal forces resulted in AuNR aggregation. After centrifuging, particles were re-suspended in aqueous CTAB-decane solution, where the molar ratio of decane to CTAB was 1.5 to generate a swelled micelle formation.[32] Under basic conditions, hydrolysis and condensation of TEOS around AuNR cores generate a mesoporous silica shell with pore diameters of roughly 4 to 5 nm and silica thickness of roughly 15 nm. More complete studies of nanoparticle pore structure and silica shell thickness, and the effects of these parameters on analyte diffusion through the pores, can be found in previous work.[34,36] After the silica coating, the resultant nanoparticles were suspended in ethanolic NH_4NO_3 under reflux to remove any residual CTAB. Considering the well-established exponential decay of the plasmonic electromagnetic fields from the gold surfaces (i.e. a decay length of roughly 2 nm[33]), we hypothesized that this CTAB-removal step via ion-exchange is critical for efficient analyte adsorption and SERS signal appearance. The UV-vis extinction spectra in Figure 1d show a ~23 nm blue-shift of the LSPR after purification. Previous literature suggests that addition of the silica shell on gold induces a red-shift in LSPR extinction, because the refractive index of silica is higher than that of standard solvents.[25,34] However, in most of these published studies, extinction measurements were made without complete CTAB removal, as we accomplished via ion-exchange, and it is likely that residual CTAB remained within the nanoparticle mesopores.

Thus, we assume that the literature-reported red-shift in LSPR extinction is attributable to the collective refractive index change of residual CTAB and the silica coating. Like the work presented herein, there are previous studies showing a blue-shift in LSPR extinction after CTAB removal.[35,36] Furthermore, a recent study demonstrated that enlarged mesopores within a silica shell enable more aqueous solvent to permeate the shell, and thus surround the gold core.[37] From these observations, we infer that the lower density of the silica in our substrate and the ion-exchange step during purification enable efficient removal of CTAB molecules and more access of bulk aqueous media near the gold, resulting in a blue-shift in LSPR extinction compared to CTAB-stabilized AuNRs. This complete CTAB removal and the added silica shell with large pores results in a comparatively large LSPR red-shift upon adsorption of a new organic molecule (BPE), which will be discussed in the following section. Figure 1b and 1c show TEM images of synthesized and purified AuNRs@mSiO_2-TMS. Both images reveal monodisperse particles with obvious mesoporous silica shell structures. In some cases, the silica shell was further modified with a small hydrophobic molecule, chlorotrimethlysilane (TMS). The zeta potentials of AuNRs@mSiO_2 and AuNRs@mSiO_2-TMS are depicted in Figure 1e. Before coating, AuNRs have a zeta potential of ~ +40 mV imbued by the CTAB bilayers. After coating with silica, both nanoparticles present negative zeta potentials, attributable to the silanol groups on the silica surface. Nanoparticles modified with TMS display a less negative zeta potential, shifted from -50 to -24 mV, indicating that condensation of hydrophobic silanes reduces the number of silanol groups at the surface.

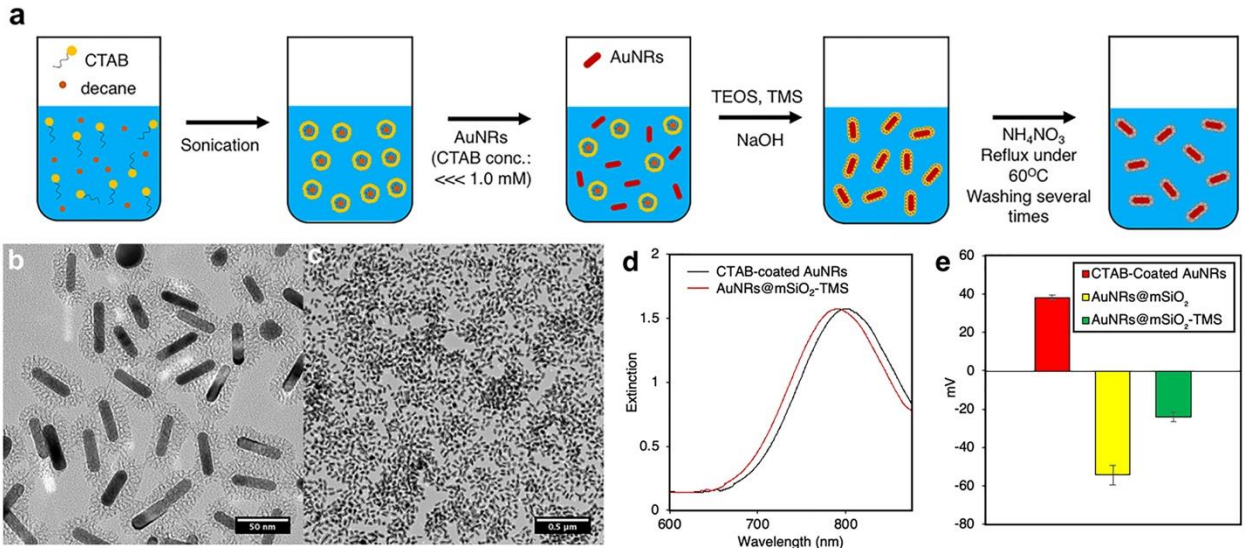

Figure. 1 AuNRs@mSiO$_2$-TMS scheme for synthesis and characterization. (a) The synthetic pathway for AuNRs@mSiO$_2$-TMS. (b-c) Representative TEM images of AuNRs@mSiO$_2$-TMS. (d) UV-vis spectra of the aqueous suspensions of CTAB-coated AuNRs (black) and AuNRs@mSiO$_2$-TMS (red) after synthesis and purification. (e) Zeta potentials of CTAB-coated AuNRs, AuNRs@mSiO$_2$, and AuNRs@mSiO$_2$-TMS. The error bars represent the standard deviation from 5 replicate measurements.

Effect of silica shell property in colloidal SERS system

The environment around the gold core in AuNRs@mSiO$_2$-TMS can be divided into 3 different regions: the silica shell, the molecules adsorbed onto the gold, and the bulk solvent. We hypothesized that all 3 components would affect the access and adsorption of BPE onto the metal core. To investigate the effect of molecular functionalization of the mesoporous silica shell first, a series of SERS experiments were performed using 1,2-di(4-pyridyl)ethylene (BPE) as an analyte. First, 10 μL of 1.5 mg/mL substrate suspensions were added to 110 μL of 1 ppm BPE solution, and the aliquots of the mixtures were transferred for SERS measurement at various time points (Figure S2). Three characteristic vibrational modes of BPE were monitored throughout these experiments, including those at 1201, 1608 and 1638 cm^{-1} shift, corresponding to a C=C

stretching mode, an aromatic ring stretching mode, and an in-plane ring mode, respectively.[38,39] As shown in Figure S2, the two spectral features at 1608 and 1638 cm^{-1} shifts are of particular interest throughout this research as these features are far from any other non-BPE background Raman signals in our experimental set up. In Figure 2, it is clear that the SERS signal intensities from BPE increase as incubation time increases. The Raman bands approach their maximum intensity after approximately 12 hours of incubation and likely decreases after that based on small shifts in substrate plasmonic properties. Even though neither mixture was shaken or sonicated, both substrates showed time-dependent signal enhancement behaviors. Not only did signals from AuNRs@mSiO_2-TMS demonstrate more intensity increments between each measurement time, but the maximum intensities from AuNRs@mSiO_2-TMS were about 2-fold higher than those of AuNRs@mSiO_2. This result suggests that the total amount of BPE on the gold surface for AuNRs@mSiO_2-TMS was higher than that of AuNRs@mSiO_2. It is likely that these improved signals from AuNRs@mSiO_2-TMS can be attributed to the added small hydrophobic trimethylsilyl groups, which are condensed not only on the outer surfaces of the shells, but also on the inner walls of the silica shell pores. Clearly, with more favorable hydrophobic interaction between the substrate and analyte,[40,41] the TMS surface modification impacted the equilibrium by preconcentrating BPE molecules close to gold core.

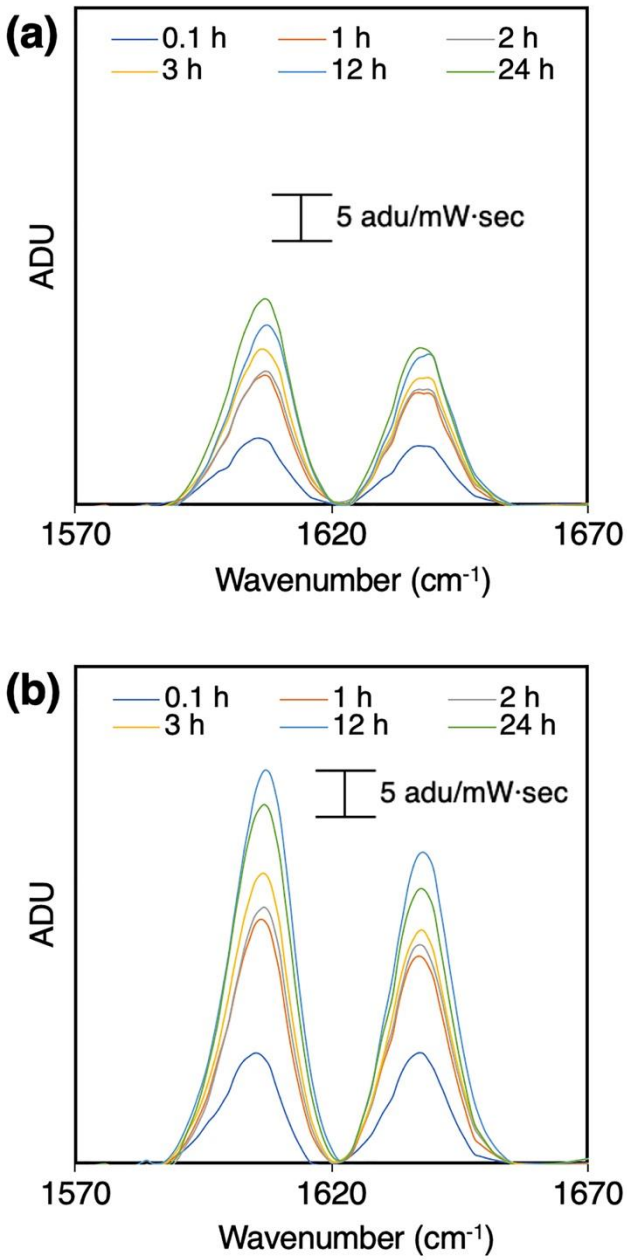

Figure 2. Colloidal SERS spectra of mixtures of 10 μL 1.5 mg/ml substrates and 110 μL of 1 ppm of BPE in water as a function of incubation time (final mixture BPE concentration: 5.0×10^{-6} M). No shaking or stirring was performed over the time course of the experiment. The spectra were baseline corrected. (a) AuNRs@$mSiO_2$ substrate and (b) AuNRs@$mSiO_2$-TMS substrate.

Not only the chemical functionalities, but also the physical properties of the silica shell can be tuned to enhance the accessibility of the analytes to the metal cores. In previous work, our group found that mesopore size can significantly affect the resulting Raman

signals, as only molecules small enough to pass through the pores in the silica shell were able to adsorb on the plasmonic cores.[30] In a similar way, we were curious if the change in pore size can affect the overall SERS signal magnitude for a given analyte. Because the pores in the silica shell are the passage for analyte access to the gold core, a larger pore size might enable more BPE access and adsorption. However, the detailed directional morphology of the pores and available LSPR surface upon the change in pore size were not obvious. Even if the pore size become larger, the possibility that an altered pore direction limits access and that the final available metal surface area doesn't change, must be considered. As shown in Figure 3, two types of AuNRs@mSiO_2-TMS (with/without decane) were prepared and added into the same BPE concentration solution separately. TEM images clearly show enlarged pore sizes when decane was added during micelle formation. The decane can function as an oil phase in aqueous media, and the small amount of decane can be surrounded by CTAB surfactant, resulting in enlarged micelle formation compared to CTAB-only micelles.[32] The BPE Raman signal intensities were always higher for the mixture of the substrate with enlarged pores at all measured time points. From this result, we can conclude that, at least within this size regime, the pore size within the silica shell directly impacts the amount of analyte that has access to the substrate cores. However, from this experiment it is not possible to determine if the enhanced signal is due to increased area of the adsorption-available Au surface, more efficient through-mesopore transport, or both. It is possible that BPE molecules passing through the shell might adsorb on the pore wall, blocking access for other BPE molecules; this situation would be more likely to occur with the smaller pore size. Thus, the enhanced SERS signal magnitude with the larger diameter pore substrates could be due to

mitigating that blocking process.

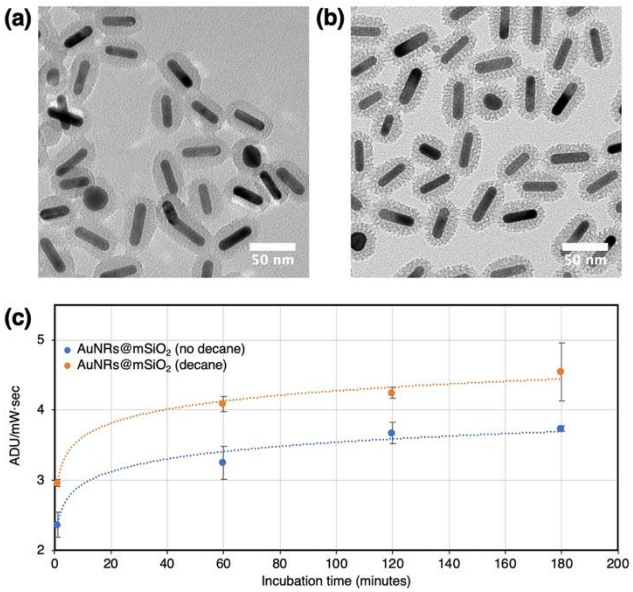

Figure 3. (a) TEM images of AuNRs@mSiO$_2$-TMS (no decane added, smaller mesopores) (b) TEM images of AuNRs@mSiO$_2$-TMS (decane added, larger mesopores) (c) Time-dependent SERS signal intensities at 1608 cm^{-1} shift from the mixtures of BPE/AuNRs@mSiO$_2$-TMS (no decane added: blue) BPE-AuNRs@mSiO$_2$-TMS(decane added: orange). The SERS was measured with the mixture of 10 μL 1.0 mg/mL substrates and 110 μL of 100 ppb of BPE in water (final mixture BPE concentration: 5.0 × 10^{-7} M). The full spectra are available in Figure S3. The dotted lines show the logarithmic fitted lines for the data points of each mixture. The error bars represent the standard deviation from three independent measurements.

Effect of CTAB molecules in colloidal SERS system

We also considered that the presence/absence of the structure-directing CTAB molecules within the shell pores or adsorbed on gold could impact the performance of the colloidal SERS system. To evaluate the impact of CTAB, we dissolved BPE in pure water,

and three different concentrated substrate suspensions were prepared: 1mM CTAB-stabilized AuNRs, 10 mM CTAB-stabilized AuNRs, and CTAB-free AuNRs@$mSiO_2$-TMS. Then, each suspension was mixed into a BPE solution of the same concentration, and UV-Vis extinction and SERS spectra were measured at different time points during incubation. The purpose of the extinction measurements was to observe any LSPR change due to the adsorption of BPE. As shown in Figure 4a, the concentrated 1mM CTAB-stabilized AuNRs suspension showed a drastic decrease in extinction at 798 nm after the suspension was added to the BPE solution. In the BPE-AuNRs mixtures, the CTAB concentration dropped from 1 mM to 67 μM. In such a case, the AuNRs would be de-stabilized, and this destabilization was accelerated upon the BPE adsorption, as the sites occupied by BPE will disturb the CTAB bilayer. Compared to this dramatic change in LSPR, the UV-Vis spectra from 10 mM CTAB-stabilized AuNRs didn't show such change in LSPR, but maintained the original extinction from the gold core (Figure 4b). In this case, the CTAB concentration decreased from 10 mM to 670 μM, and this concentration was still high enough to protect the gold from dissolution or aggregation. For the BPE/AuNRs@$mSiO_2$-TMS mixture, even though there was no CTAB present, the silica shell maintained the LSPR extinction as in the 10 mM CTAB-stabilized AuNR mixture (Figure 4c). However, in the SERS spectra, the two apparently stable mixtures showed significant spectral differences (Figure 4d). Unlike the 10 mM CTAB-stabilized AuNR mixture where very low magnitude BPE Raman signals are measured even after long incubation, the BPE/AuNRs@$mSiO_2$-TMS mixture showed clear and high intensity SERS BPE signals, even higher than that of the BPE/1mM CTAB-stabilized AuNR mixture. Furthermore, when the BPE concentration was high, only the AuNRs@$mSiO_2$-

TMS mixture showed a significant LSPR red-shift from 775 nm to 798 nm (Δ λ = 23 nm, Figure S4). This red-shift is due to the high concentration and adsorption of BPE to gold cores, resulting in a significant change in local refractive index,[42] indicating much more enhanced accessibility of BPE to the gold core when CTAB has been removed by purification. This experiment shows that the silica shell not only promotes colloidal stability, but also facilitates aqueous BPE access compared to AuNRs with CTAB bilayer-based protection.

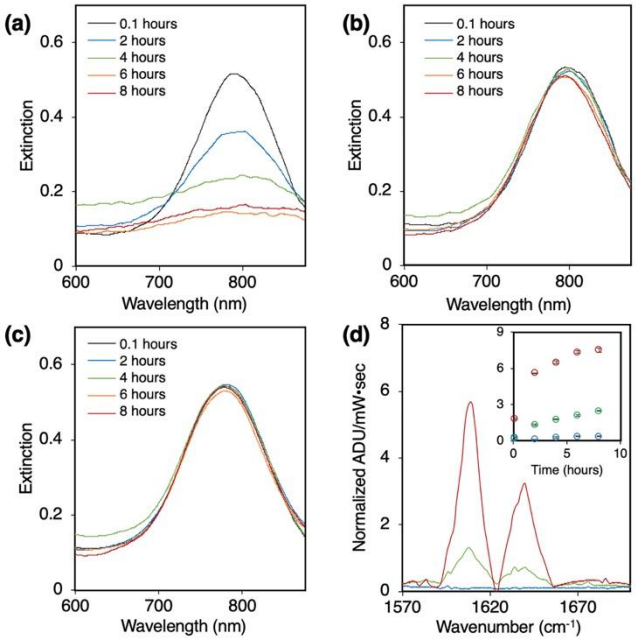

Figure 4. (a) Time-dependent extinction spectra of the mixtures of an aliquot of the concentrated suspensions of 1 mM CTAB-coated AuNRs and 50 ppb BPE solution. (b) Time-dependent extinction spectra of the mixtures of an aliquot of the concentrated suspensions of 10 mM CTAB-coated AuNRs and 50 ppb BPE solution. (c) Time-dependent extinction spectra of the mixtures of an aliquot of the concentrated suspensions of AuNRs@mSiO_2-TMS and 50 ppb BPE solution. (d) SERS spectra of BPE/AuNR mixtures: (red) AuNRs@mSiO_2-TMS, (green) 1 mM CTAB-coated AuNRs, and (blue) 10 mM CTAB-coated AuNRs after 2 hours of incubation. For all mixtures, BPE concentration was 50 ppb and AuNR concentration was 2.0 mg/mL. (Final mixture BPE concentration: 2.5×10^{-7} M, Inset: the time dependent SERS signal intensities from three mixtures at 1608 cm^{-1} shift.)

Effect of bulk solvent property on colloidal SERS system: ionic strength

As can be seen in Figures 3 and 4, the chemical and physical properties of the silica shell can affect the intensity of SERS signals and enable more efficient interaction between BPE and AuNRs than conventional CTAB layers in colloidal state. With this in mind, we wanted to explore how the properties of the solvent can influence analyte-substrate interaction. In our colloidal SERS system, both substrates and analytes were dispersed, and the characteristics of the bulk solvent can impact their colloidal properties and thus, SERS signals. Previously (in Figure 1e), we saw that TMS modification induced a change in the zeta potential toward less negative values. This change might enable more favorable approach of hydrophobic BPE to the shell. As an alternate approach to achieve the same goal, we considered the widely known fact that increasing the aqueous ionic strength screens the zeta potential of the silica shell. To investigate the zeta potential screening effect explicitly, BPE molecules were dissolved in aqueous solutions of 200 mM sodium chloride, ammonium acetate, or lithium perchlorate, and salt-free water to obtain four different 50 ppb BPE solutions. The colloidal SERS spectra from these solutions were measured with AuNRs@mSiO_2-TMS as SERS substrates. Figure 5 shows SERS spectra of BPE scattering features in the 1550 to 1700 cm^{-1} shift range at three different incubation time points. No observable signals were measured immediately following dispersion in any of the four mixtures, but after 30 mins and 60 mins of incubation, it was clear that BPE in all three aqueous solutions with higher ionic strengths

showed more enhanced signal intensities than BPE in salt-free water. Interestingly, Raman signals in the NaCl solution were much more intense than the signals from other salt solutions, likely due to chloride activation; chloride anion is known to adsorb onto the colloidal metal surface and enhance the Raman signal intensities of certain single molecules, such as pyridine.[43–45] However, considering that other anions are not known for the similar activation, and that perchlorate especially has extremely weak affinity for gold surfaces,[46,47] the zeta potential screening effect that draws hydrophobic molecules appears influential on enhancing Raman signal intensities in this colloidal SERS system.

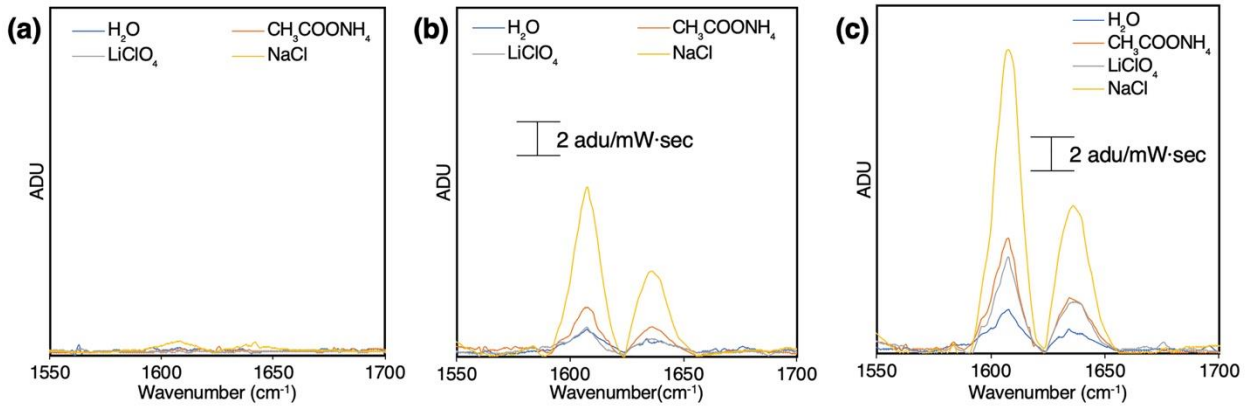

Figure 5. (a) SERS spectra of BPE and AuNRs@mSiO$_2$-TMS mixtures, focused on scattering features at 1608 and 1638 cm^{-1} shift. Each mixture had 200 mM of the identified salt during incubation, except for the salt-free water control. The spectra were taken right after 10 µL of 1.5 mg/mL AuNR@SiO$_2$-TMS was added to each 110 µL 50 ppb aqueous BPE solution. (b) 30 mins after mixing. (c) 60 mins after mixing (final mixture BPE concentration: 2.5 × 10^{-7} M).

Effect of bulk solvent on colloidal SERS system: temperature and solvent

We also investigated how varying temperature of the bulk solvent impacted the performance of the colloidal SERS system. Initially, we wanted to observe the diffusion

and adsorption behaviors of the BPE separately to characterize which was the more critical step for achieving high intensity SERS spectra. First, we systematically studied the effects of incubation temperature. We hypothesized that more rapid Brownian motion of the substrates and analytes would result in more effective diffusion of the analyte to the substrate cores. BPE/colloidal substrate mixtures were prepared as they were in the previous experiment. Each mixture was then incubated at a different temperature: 6, 23, 32, or 55 °C for 10 minutes. The incubation time was limited to several minutes as the high temperature might affect the properties of the AuNRs with longer incubation times. From our UV-Vis spectra, we concluded that the LSPR change due to 10 minute incubation is minimal at all temperatures (Figure S7). As shown in Figure 6, the Raman spectra clearly display more enhanced signal intensities when the mixtures were incubated at higher temperatures. Compared to the sample kept at room temperature for incubation, incubation at lower temperature might lead to slower diffusion while higher temperature induced more rapid diffusion and increased interactions between the substrates and the analytes. However, attributing enhanced Raman intensities only to rapid diffusion might be too simplified an answer, as temperature can affect many factors such as adsorbed analyte arrangement and mutual interactions, metal-adsorbate interactions, and Fermi distribution of electrons.[48,49]

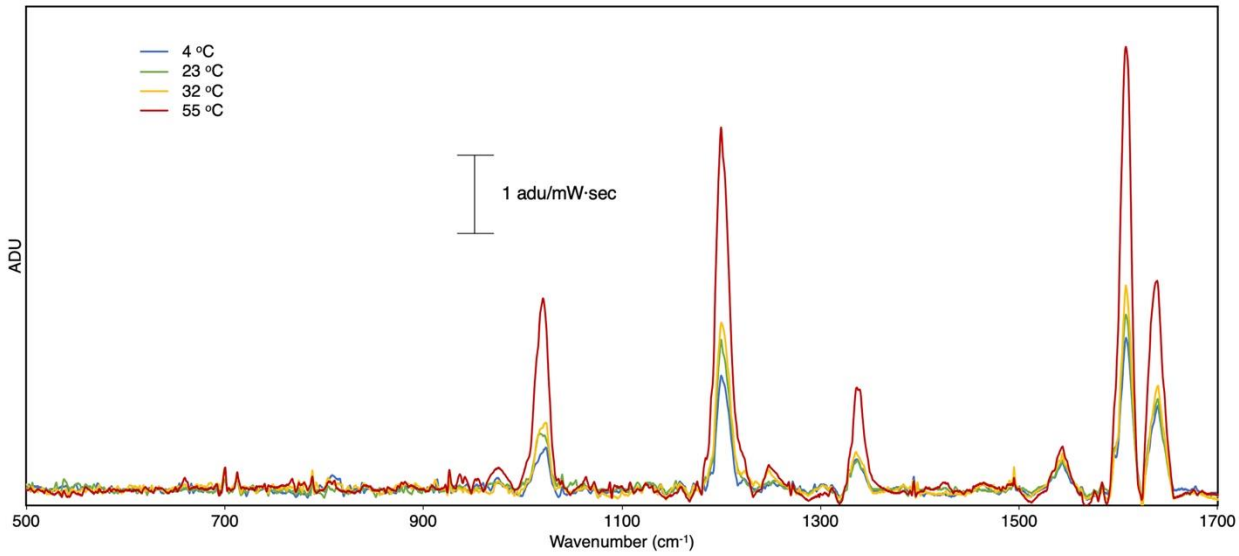

Figure 6. SERS spectra of BPE and AuNRs@mSiO$_2$-TMS mixtures, incubated in four different temperatures for 10 minutes after the mixing. The mixture was formed by mixing 10 μL of AuNRs (1.5 mg/mL) to 110 μL of 50 ppb BPE solution (final mixture BPE concentration: 2.5×10^{-7} M).

To follow up, we used the same four temperatures but modified the procedure (Scheme 1a). First, we centrifuged and re-dispersed the mixtures before the incubation in different temperatures to remove residual BPE in solution (Scheme 1b). Thus, no further diffusion through the pores occurred during incubation in different temperature. Second, only AuNRs@mSiO$_2$-TMS suspensions were incubated in different temperatures before being mixed with BPE to see if any change in gold cores affect the measured SERS spectra (Scheme 1c). As shown in Figure 7b and 7c, compared to the control experiment in Figure 7a, no Raman signal magnitude difference among different incubation temperatures was observed. This result reveals that the enhanced SERS intensity in higher temperature wasn't from any change in the gold surface. More importantly, from Figure 7b, it is clear that the BPE molecules already adsorbed onto the

metal didn't make a difference in Raman signal intensity even though the mixtures were incubated in different temperatures. However, it still wasn't clear at this point whether the higher SERS signal intensity was mainly caused by more rapid diffusion or more facile adsorption of BPE.

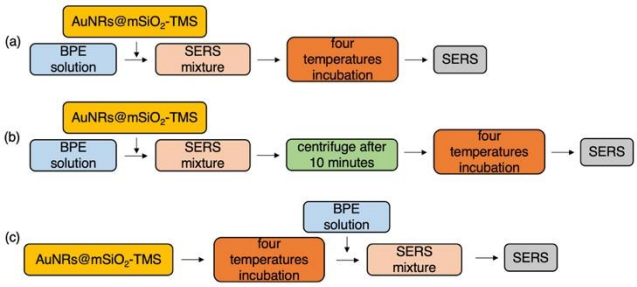

Scheme 1. Three experimental schemes to confirm that the enhanced SERS signal intensities in higher temperature incubation were caused by increased amount of BPE adsorbed on the surface rather than by different chemical interaction between substrate and analyte or change in the substrate itself.

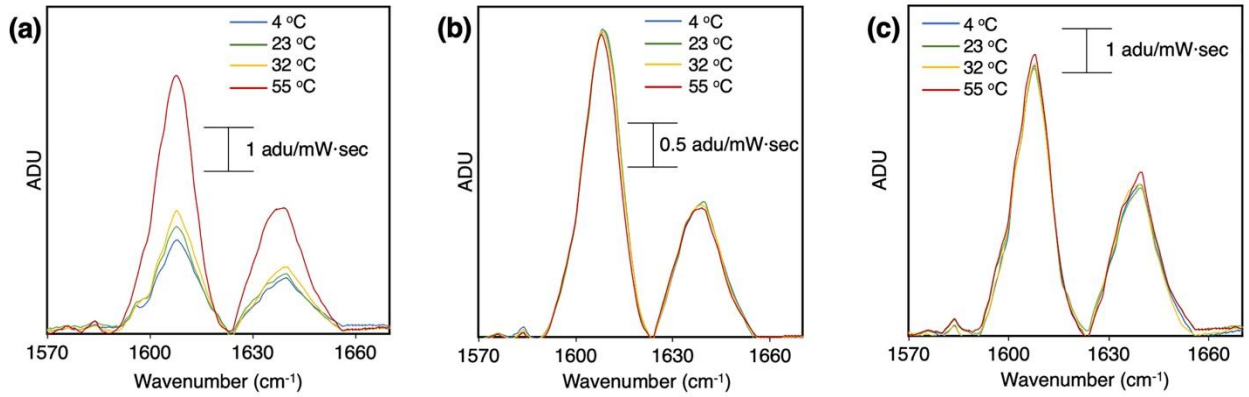

Figure 7. (a) SERS spectra of BPE and AuNRs@mSiO$_2$-TMS mixtures, focused on scattering features at 1608 and 1638 cm^{-1} shift from Scheme 1a. (b) SERS spectra of BPE and AuNRs@mSiO$_2$-TMS mixtures, focused on scattering features at 1608 and 1638 cm^{-1} shift from Scheme 1b. (c) SERS spectra of BPE and AuNRs@mSiO$_2$-TMS mixtures, focused on scattering features at 1608 and 1638 cm^{-1} shift from Scheme 1c. All samples were formed by mixing 10 μL of AuNRs (1.5 mg/mL) to 110 μL of 50 ppb BPE

solution (final mixture BPE concentration: 2.5×10^{-7} M).

To observe the effect of diffusion more clearly, we used the binary solvent system of glycerol and water. The two solvents are miscible but possess very different viscosity of 934×10^{-3} Pa·s and 0.89×10^{-3} Pa·s, respectively. Correspondingly, the two solvents show very different diffusion coefficients: 0.014×10^{-9} m^2/s for glycerol and 1.025×10^{-9} m^2/s for water (the values were obtained from mutual diffusion coefficient calculation and extrapolation from previous literature).[50] We expected that both BPE and AuNRs@mSiO$_2$-TMS would diffuse much more slowly in glycerol than water, and this would give us more insight regarding the relationship between the diffusion behavior of BPE and the SERS signal intensity. First, we assessed whether or not mechanical agitation could expedite diffusion. In one experiment, two of the same BPE and AuNR@SiO$_2$-TMS mixtures in pure water were prepared, and one of the mixtures was stirred with a magnetic bar. In Figure S6, the plots of the time-dependent SERS signal intensities at 1608 cm^{-1} shift from the two mixtures were nearly identical, and this indicates that in pure water, mechanical agitation didn't improve the diffusion. The result was expected, as in water, both the analytes and the substrates were homogeneously dispersed in our colloidal SERS system, and this homogeneous dispersion in bulk solution would be maintained even with the agitation. Thus, the stirring would move the entire analyte and substrate and not alter the rate of diffusion through the pores.

To observe the diffusion behaviors of the substrates and analytes more clearly, we generated an extreme solution condition by preparing a binary system. In this experiment, we prepared a concentrated AuNRs@mSiO$_2$-TMS suspension in glycerol, and these suspensions were added to several vials first (Scheme 2 inset photo). Then, aqueous BPE solutions were added to the vials. We found that upon the BPE solution addition, due to the miscibility between glycerol and water, the mixtures became visually homogenous quickly. For half of the prepared vials, we added stir bars and stirred the mixtures for 10 minutes of incubation, and the rest of the vials remained unstirred while the mixtures were incubated at four different temperatures. The results in Figure 8 show that in all temperature conditions, the BPE SERS signal magnitudes for the stirred mixtures were higher than that of the non-stirred mixtures. The agitation in this set-up helped more rapid diffusion of glycerol into water, resulting in faster diffusion of AuNRs@mSiO$_2$-TMS to the BPE solution and more frequent contact between the analyte and the substrate. When comparing the mixtures incubated in varied temperatures, the stirring condition induced more significant changes in the SERS signal intensity compared to those that were not stirred. Because of the high viscosity of glycerol, one would expect the stirring to have a larger impact than temperature change in terms of expediting diffusion. In a previous experiment, Tripathi et al. showed that in a low temperature environment, where diffusion is limited, stirring significantly enhanced the SERS signal intensity for thiophenol adsorbed on gold, and the saturation occurred roughly 25 times faster than in an unstirred solution.[51] It is important to note, however, that in their SERS system, the gold substrate was stationary so the stirring would be more impactful for the

contact between the analyte and substrate. Similarly, in our experimental condition, the signal intensities from the unstirred mixtures in each condition were still higher than those of the stirred mixtures in the next lower temperatures. Considering the high viscosity of the glycerol and effect of mechanical agitation in this binary condition, it is sensible that the agitation should affect the diffusion rates more than temperature. Thus, we speculate that rather than diffusion, a thermodynamic factor is more critical for acquiring higher SERS intensities. With the results measured here, it is reasonable to argue that in our colloidal substrate-analyte interaction, the diffusion of BPE through the silica mesopores is not likely a critical step for the SERS signal production compared to adsorption. Concurrently, the higher SERS signal magnitude for the mixtures incubated in higher temperature is more likely to be related to more efficient adsorption (physisorption) and the activation energy of chemisorption. Based on the results shown here, it is fair to argue that the higher temperature helped BPE to overcome the activation energy required to chemically adsorb onto the gold surface, resulting in increased SERS signal intensities.[51] Thus, the hypothesized delayed diffusion rates due to the silica shell intervention between BPE and the gold core seems minimal or negligible, compared to the chemical adsorption of BPE for the production of the SERS signal.

To support our hypothesis, we've analyzed the peak area ratio of the peak at 1608 cm^{-1} shift to the peak at 1638 cm^{-1} shift at each temperature. A previous study shows that this ratio depends on the fraction of BPE molecules bound to the gold surface.[52] The authors state that the BPE vibrational mode at 1608 cm^{-1} shift exhibits a larger deformation potential and a stronger chemical coupling to the metal, and it is enhanced more than the 1638 cm^{-1} shift mode. Thus, the increased ratio values indicate an

increased molar fraction of BPE molecules bound to the gold over total BPE molecules observed in Raman spectra. The experimentally obtained ratios from our results show that the ratio is temperature-dependent: higher temperature induced a higher ratio. Thus, it is reasonable to argue that the binding between BPE molecules and the gold cores were favored at higher temperatures, where the chemical interaction is favored. It appears that chemical binding between BPE molecules and the gold surface is the more critical factor for achieving improved Raman intensity, compared to simply locating BPE molecules near the gold surface via diffusion through silica shell pores. The unstirred mixtures showed smalled ratio values than the stirred samples but this difference was not statistically significant.

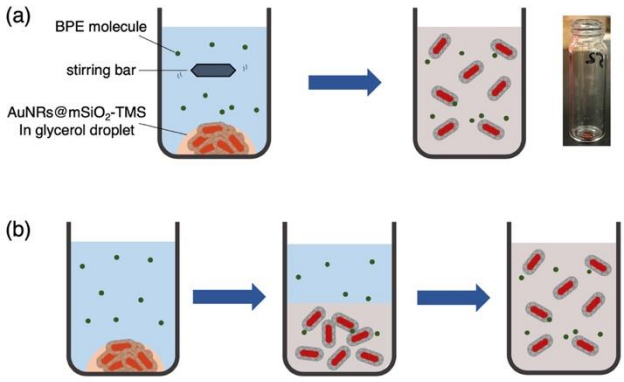

Scheme 2. Schematic description of the mixtures of aqueous BPE solution and AuNRs@mSiO$_2$-TMS in glycerol incubation with (a) stirring (rapid diffusion) and (b) non-stirring (slow diffusion).

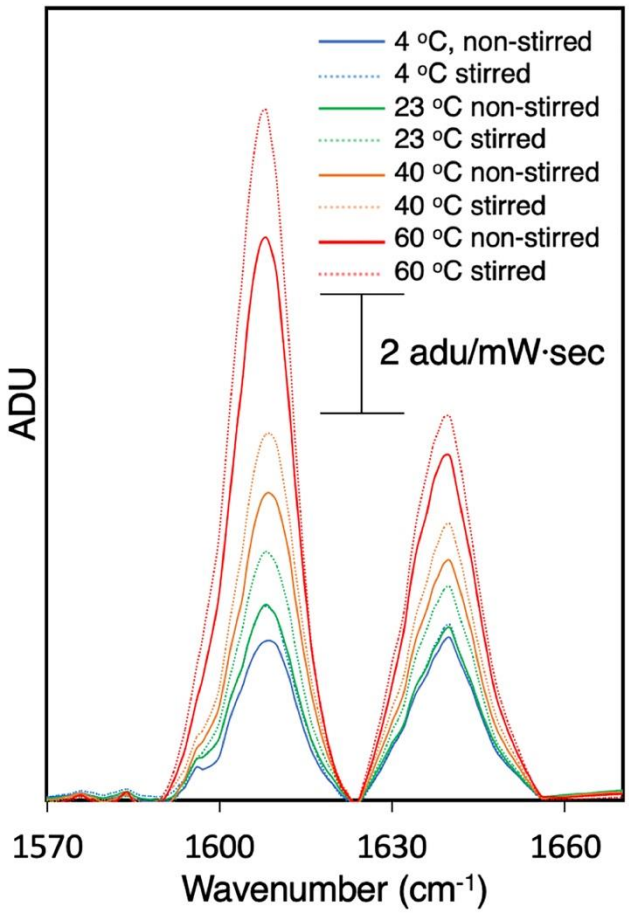

Figure 8. SERS spectra of the mixture of aqueous BPE solution and AuNRs@mSiO$_2$-TMS glycerol droplet, focusing on scattering features at 1608 and 1638 cm^{-1} shift after 10 minute incubation in four different temperatures. For each temperature, the mixtures were not stirred (solid line) or stirred (dotted line) during the incubation. The spectra were measured after 10 minutes of incubation, following the mixing of 20 µL of 6.0 mg/mL AuNR@SiO$_2$-TMS in glycerol and 1 mL 50 ppb aqueous BPE solution (final mixture BPE concentration: 2.7 × 10^{-7} M).

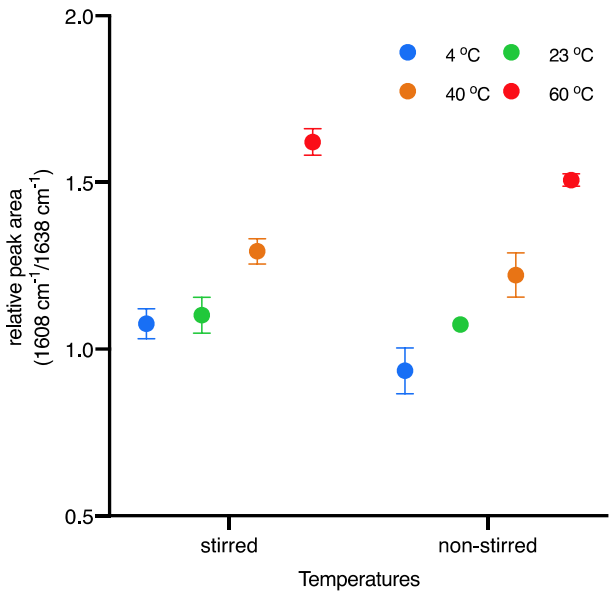

Figure 9. Relative peak area ratios (1608 /1638 cm^{-1} shift) of the mixtures of aqueous BPE solution and AuNRs@mSiO_2-TMS in glycerol droplets after 10-minute incubation in four different temperatures. The experimental conditions were the same as in Figure 8. The error bars represent the standard deviation from three independent measurements.

From the previous experiment, it appeared that the adsorption of BPE onto the gold surface was more critical than diffusion. To verify this deduction, we hypothesized that even in a set of solvents with varying volume ratio of glycerol in water at a given temperature, where both the analyte and substrates would diffuse more slowly with increasing volume percentage of glycerol, we would still measure similar SERS signal magnitudes for all samples. This binary system, depending on the volume percentage of glycerol, has different diffusion coefficient values.[53] We prepared five different solvent conditions (water only, 30% glycerol, 50% glycerol, 70% glycerol, and 90% glycerol by volume) to investigate if the solvent conditions and varied viscosities affect the molecular diffusion behaviors and resulting SERS intensities. We focused on the peak area at 1608 cm^{-1} shift from each mixture, and the data were collected at different time points for 10

hours. The absolute peak area showed that increased volume of glycerol in the solvent caused lower BPE signal intensities (Figure 10a). This phenomenon can be explained by three factors. First, the increased viscosities and the resulting diffusion rates limited the number of BPE molecules on the gold surface in each solvent condition. Second, the solvents with more glycerol have higher solubility for BPE than water, thus more BPE molecules will be dissolved in the solvent than on the substrate surface in final equilibrium state. Last, adsorbed glycerol on the gold surface resulted in a less BPE adsorption on the surface. Our interest was the effect of diffusion on the time-dependent SERS spectra, not the absolute peak intensities. Thus, the peak area at different time points was divided by the maximum peak area in each condition. The normalized relative peak area for 10 hours showed the adsorption behaviors of the analytes on the substrates (Figure 10b). The mixture of 90% glycerol was omitted as no relevant BPE peaks were observed during the measurement. In previous literature, researchers have investigated the diffusion behaviors of small molecules through mesoporous silica in different conditions, such as varied solvents,[54] varied pH of media,[55] varied hydrophobicity of the molecules,[56] and in a hybrid microsphere structure[57] with appropriate transport models. Herein, we assume that the BPE molecules occupy each site on the gold surface via chemical binding. We used a simplified Prout−Tompkins model to evaluate the first-order chemical kinetics:[51]

$$y = \left(1 - e^{-k(t)}\right) \quad (1)$$

where y is fraction of bound BPE, t is the incubation time, and k is the binding association rate constant.

Thus, when the temporal data points were fitted using equation (1), all mixtures

showed Langmuir-type association plots. The acquired rate constants can be found in Table 1. The trend in rate constants among different solvent conditions shows that the higher glycerol percentage led to lower rate constant values, even though the differences were small, especially when the viscosities for different solvents were considered. This indicates that the contribution of diffusion rates on the Raman signal intensity in this colloidal SERS platform is minimal. We were also curious if there is a difference in the rate for the chemical binding when BPE is dispersed in different solvents. Similar to Figure 9, the peak area ratio of 1608 cm^{-1} shift to 1638 cm^{-1} shift at each time point was obtained and normalized by the maximum ratio in all conditions (Figure 10c and 10d). Interestingly, the trend was opposite to Figure 10b: the acquired rate constants increased as the glycerol percentage went up. This result suggests that when there is more glycerol, the system more rapidly reaches the equilibrium state for BPE binding to the gold surface. We speculate that this occurs because the solubility of BPE is higher in glycerol than in water, thus among BPE molecules near the gold surface, the molar faction of BPE adsorbed on gold is lower with higher glycerol percentages in the glycerol/water mixture. When the results from Figure 10b and Figure 10d are combined, it is clear that the effect of diffusion rates varied via solvent composition is not substantial for determining the Raman signal magnitude.

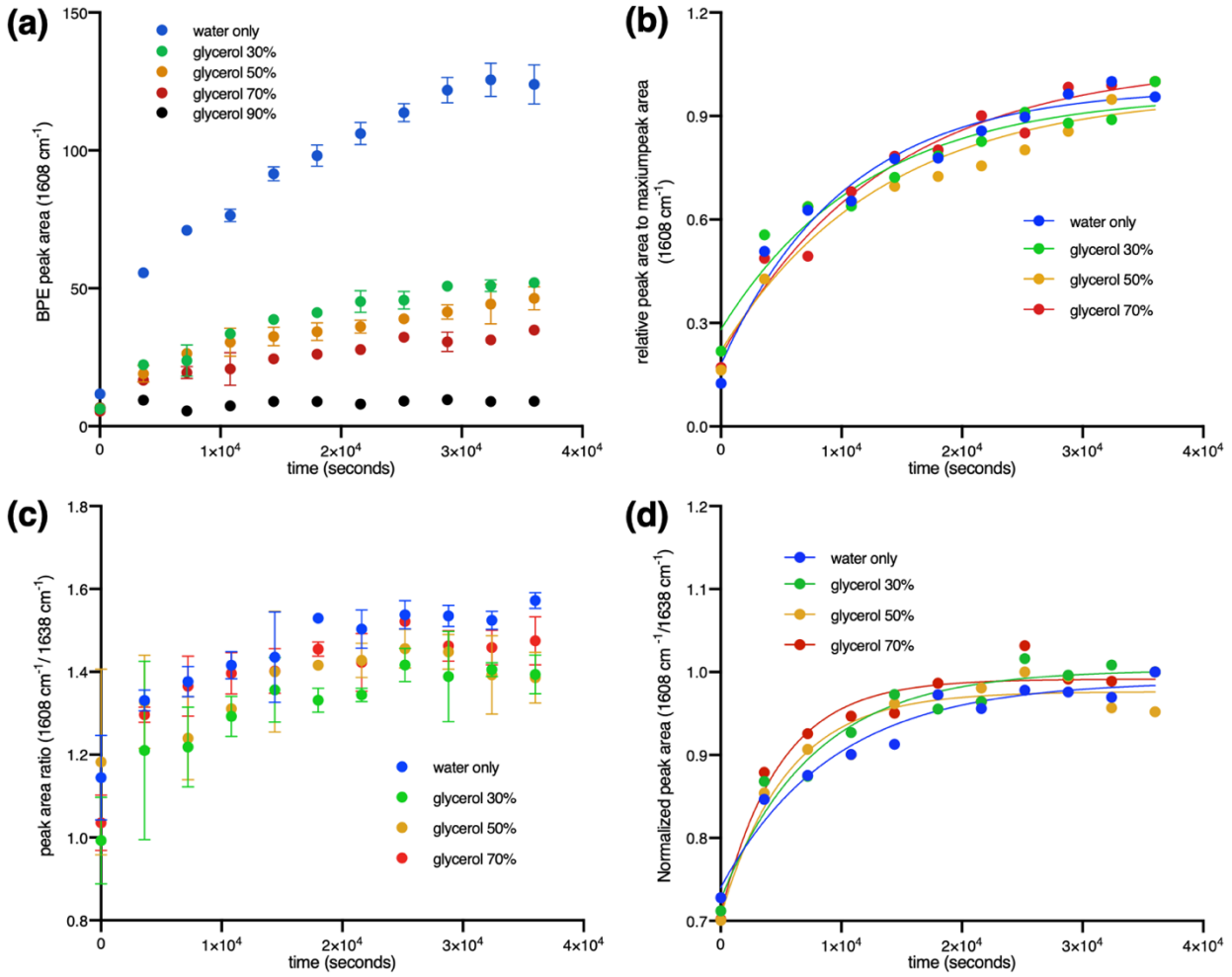

Figure 10. (a) Time-dependent absolute BPE SERS peak area at 1608 cm^{-1} shift for each mixture of BPE and AuNRs@mSiO_2-TMS in glycerol-water mixtures of varying volume ratio. (b) Time-dependent relative SERS signal peak area to that of maximum area at 1608 cm^{-1} shift in each mixture. The fitted lines for each mixture were obtained by fitting the data to equation (1). (C) Time-dependent relative peak area ratios (1608 /1638 cm^{-1} shift) of the mixtures. (d) Time-dependent relative SERS signal peak area ratios (1608 /1638 cm^{-1} shift) to that of the maximum area ratios for each mixture. The fitted lines for each mixture were obtained by fitting the data to equation (1).

	Viscosity (mPa·s)[58]	Rate constant of association (s^{-1}) (Figure 10b)	Coefficient of determination, R^2 (Figure 10b)	Rate constant of association (s^{-1}) (Figure 10d)	Coefficient of determination, R^2 (Figure 10d)
Water only	1.00	9.74×10^{-5}	0.9630	1.07×10^{-4}	0.9635
Glycerol 30%	2.50	8.29×10^{-5}	0.9412	1.31×10^{-4}	0.9517
Glycerol 50%	6.00	7.56×10^{-5}	0.9375	1.84×10^{-4}	0.9468
Glycerol 70%	22.50	7.37×10^{-5}	0.9706	2.01×10^{-4}	0.9523
Glycerol 90%	219.0	-	0.3164	-	-

Table 1. Solvent compositions, viscosities, the rate constants of associations and corresponding coefficients of determinations for each fitted line in Figure 10b and 10d. The rate constants for mixtures of 90% glycerol were not calculated due to the poor values of R^2.

Conclusion

The mesoporous silica shell coating the plasmonic metal core has proven to be an excellent protecting agent against dissolution or aggregation of the metal in colloidal SERS systems. The silica shell, however, can also be considered a potential physical barrier, hindering analyte approach to the LSPR-enhanced surface. In this work, we considered the shell as the intermediate region between the bulk solvent and the surface of the metal, and investigated the interaction between the analyte and substrates, focusing on the diffusion and adsorption through the shell. The results show that the

physical/chemical characteristics of the shell can be controlled to allow more analyte approach to the gold surface, resulting in improved SERS signal magnitudes. Compared to CTAB-based stabilizing layers, the silica shells allowed more efficient adsorption of BPE and more direct exposure of the core surface to the bulk solvent while successfully maintaining the plasmonic properties. Systematic experiments in different environmental conditions showed that the hydrophobic surface modification of the silica shell preconcentrated the analytes around the substrates via setting new equilibrium state and the screening of electric potentials on the substrates enhanced the access of the hydrophobic analytes to the gold core. In addition, variation of temperature and solvent composition strongly suggest that in colloidal SERS systems, the diffusion rate of BPE through the shells to cores is not as impactful as the adsorption process on the metal surface for the production of SERS signals.

Supporting Information

Molecular information (structure, solubility, size) of BPE, the description of SERS experimental set up, full SERS spectra of the analyte-substrate mixtures in colloidal SERS, UV-Vis extinction spectra of the analyte-substrate mixtures in different BPE concentrations and the types of the substrates, time-dependent SERS signal intensities of BPE with/without mechanical agitation, UV-Vis extinction spectra of the analyte-substrate mixtures incubated in different temperatures.

Acknowledgements

We would like to acknowledge 3M for their collaboration and funding. This work was supported by National Science Foundation under the Center for Sustainable Nanotechnology (CSN), CHE-1503408. The CSN is part of the Centers for Chemical Innovation Program. We acknowledge helpful discussion from Prof. Theresa M. Reineke and Victoria Szlag. We thank Joshua G. Hinman and Catherine J. Murphy for providing Au nanorods used in preliminary experiments for this work. Parts of this work, especially TEM characterization, were carried out in the Characterization Facility at the University of Minnesota, which receives partial support from NSF through the MRSEC program (DMR-1420013).

Reference

(1) West, J. L.; Halas, N. J. Engineered Nanomaterials for Biophotonics Applications: Improving Sensing, Imaging, and Therapeutics. *Annu. Rev. Biomed. Eng.* **2003**, *5* (1), 285–292.

(2) Astruc, D.; Lu, F.; Aranzaes, J. R. Nanoparticles as Recyclable Catalysts: The Frontier between Homogeneous and Heterogeneous Catalysis. *Angew. Chem. Int. Ed.* **2005**, *44* (48), 7852–7872.

(3) Lee, K.-S.; El-Sayed, M. A. Gold and Silver Nanoparticles in Sensing and Imaging: Sensitivity of Plasmon Response to Size, Shape, and Metal Composition. *J. Phys. Chem. B* **2006**, *110* (39), 19220–19225.

(4) Tian, B.; Zheng, X.; Kempa, T. J.; Fang, Y.; Yu, N.; Yu, G.; Huang, J.; Lieber, C. M. Coaxial Silicon Nanowires as Solar Cells and Nanoelectronic Power Sources. *Nature* **2007**, *449* (7164), 885–889.

(5) Hoener, C. F.; Allan, K. A.; Bard, A. J.; Campion, A.; Fox, M. A.; Mallouk, T. E.; Webber, S. E.; White, J. M. Demonstration of a Shell-Core Structure in Layered Cadmium Selenide-Zinc Selenide Small Particles by x-Ray Photoelectron and Auger Spectroscopies. *J. Phys. Chem.* **1992**, *96* (9), 3812–3817.

(6) Honma, I.; Sano, T.; Komiyama, H. Surface-Enhanced Raman Scattering (SERS) for Semiconductor Microcrystallites Observed in Silver-Cadmium Sulfide Hybrid Particles. *J. Phys. Chem.* **1993**, *97* (25), 6692–6695.

(7) Zhou, H. S.; Sasahara, H.; Honma, I.; Komiyama, H.; Haus, J. W. Coated Semiconductor Nanoparticles: The CdS/PbS System's Photoluminescence Properties. *Chem. Mater.* **1994**, *6* (9), 1534–1541.

(8) Oldenburg, S. J.; Averitt, R. D.; Westcott, S. L.; Halas, N. J. Nanoengineering of Optical Resonances. *Chem. Phys. Lett.* **1998**, *288* (2–4), 243–247.

(9) Laurent, S.; Forge, D.; Port, M.; Roch, A.; Robic, C.; Vander Elst, L.; Muller, R. N. Magnetic Iron Oxide Nanoparticles: Synthesis, Stabilization, Vectorization, Physicochemical Characterizations, and Biological Applications. *Chem. Rev.* **2008**, *108* (6), 2064–2110.
(10) Ghosh Chaudhuri, R.; Paria, S. Core/Shell Nanoparticles: Classes, Properties, Synthesis Mechanisms, Characterization, and Applications. *Chem. Rev.* **2012**, *112* (4), 2373–2433.
(11) Jeanmaire, D. Surface Raman Spectroelectrochemistry Part I. Heterocyclic, Aromatic, and Aliphatic Amines Adsorbed on the Anodized Silver Electrode. *J. Electroanal. Chem.* **1977**, *84* (1), 1–20.
(12) Sharma, B.; Frontiera, R. R.; Henry, A.-I.; Ringe, E.; Van Duyne, R. P. SERS: Materials, Applications, and the Future. *Mater. Today* **2012**, *15* (1–2), 16–25.
(13) Jain, P. K.; Huang, X.; El-Sayed, I. H.; El-Sayed, M. A. Noble Metals on the Nanoscale: Optical and Photothermal Properties and Some Applications in Imaging, Sensing, Biology, and Medicine. *Acc. Chem. Res.* **2008**, *41* (12), 1578–1586.
(14) Jones, M. R.; Osberg, K. D.; Macfarlane, R. J.; Langille, M. R.; Mirkin, C. A. Templated Techniques for the Synthesis and Assembly of Plasmonic Nanostructures. *Chem. Rev.* **2011**, *111* (6), 3736–3827.
(15) Gaspar, D.; Pimentel, A. C.; Mateus, T.; Leitão, J. P.; Soares, J.; Falcão, B. P.; Araújo, A.; Vicente, A.; Filonovich, S. A.; Águas, H.; et al. Influence of the Layer Thickness in Plasmonic Gold Nanoparticles Produced by Thermal Evaporation. *Sci. Rep.* **2013**, *3* (1).
(16) Li, J. F.; Huang, Y. F.; Ding, Y.; Yang, Z. L.; Li, S. B.; Zhou, X. S.; Fan, F. R.; Zhang, W.; Zhou, Z. Y.; Wu, D. Y.; et al. Shell-Isolated Nanoparticle-Enhanced Raman Spectroscopy. *Nature* **2010**, *464* (7287), 392–395.
(17) Lin, X.-D.; Uzayisenga, V.; Li, J.-F.; Fang, P.-P.; Wu, D.-Y.; Ren, B.; Tian, Z.-Q. Synthesis of Ultrathin and Compact Au@MnO2 Nanoparticles for Shell-Isolated Nanoparticle-Enhanced Raman Spectroscopy (SHINERS). *J. Raman Spectrosc.* **2012**, *43* (1), 40–45.
(18) Ma, L.; Huang, Y.; Hou, M.; Li, J.; Xie, Z.; Zhang, Z. Pinhole-Containing, Subnanometer-Thick Al_2O_3 Shell-Coated Ag Nanorods as Practical Substrates for Quantitative Surface-Enhanced Raman Scattering. *J. Phys. Chem. C* **2016**, *120* (1), 606–615.
(19) Yang, D.; Xia, L.; Zhao, H.; Hu, X.; Liu, Y.; Li, J.; Wan, X. Preparation and Characterization of an Ultrathin Carbon Shell Coating a Silver Core for Shell-Isolated Nanoparticle-Enhanced Raman Spectroscopy. *Chem. Commun.* **2011**, *47* (20), 5873.
(20) Fan, W.; Lee, Y. H.; Pedireddy, S.; Zhang, Q.; Liu, T.; Ling, X. Y. Graphene Oxide and Shape-Controlled Silver Nanoparticle Hybrids for Ultrasensitive Single-Particle Surface-Enhanced Raman Scattering (SERS) Sensing. *Nanoscale* **2014**, *6* (9), 4843–4851.
(21) Lum, W.; Bruzas, I.; Gorunmez, Z.; Unser, S.; Beck, T.; Sagle, L. Novel Liposome-Based Surface-Enhanced Raman Spectroscopy (SERS) Substrate. *J. Phys. Chem. Lett.* **2017**, *8* (12), 2639–2646.

(22) Xu, L.-J.; Zong, C.; Zheng, X.-S.; Hu, P.; Feng, J.-M.; Ren, B. Label-Free Detection of Native Proteins by Surface-Enhanced Raman Spectroscopy Using Iodide-Modified Nanoparticles. *Anal. Chem.* **2014**, *86* (4), 2238–2245.
(23) Amstad, E.; Textor, M.; Reimhult, E. Stabilization and Functionalization of Iron Oxide Nanoparticles for Biomedical Applications. *Nanoscale* **2011**, *3* (7), 2819.
(24) Lin, Y.-S.; Abadeer, N.; Hurley, K. R.; Haynes, C. L. Ultrastable, Redispersible, Small, and Highly Organomodified Mesoporous Silica Nanotherapeutics. *J. Am. Chem. Soc.* **2011**, *133* (50), 20444–20457.
(25) Wu, W.-C.; Tracy, J. B. Large-Scale Silica Overcoating of Gold Nanorods with Tunable Shell Thicknesses. *Chem. Mater.* **2015**, *27* (8), 2888–2894.
(26) Gao, Z.; Ring, H. L.; Sharma, A.; Namsrai, B.; Tran, N.; Finger, E. B.; Garwood, M.; Haynes, C. L.; Bischof, J. C. Scalable Silica-Coated Iron Oxide Nanoparticles for Nanowarming in Regenerative Medicine. *submitted.*
(27) Abadeer, N. S.; Brennan, M. R.; Wilson, W. L.; Murphy, C. J. Distance and Plasmon Wavelength Dependent Fluorescence of Molecules Bound to Silica-Coated Gold Nanorods. *ACS Nano* **2014**, *8* (8), 8392–8406.
(28) Zhang, Z.; Wang, L.; Wang, J.; Jiang, X.; Li, X.; Hu, Z.; Ji, Y.; Wu, X.; Chen, C. Mesoporous Silica-Coated Gold Nanorods as a Light-Mediated Multifunctional Theranostic Platform for Cancer Treatment. *Adv. Mater.* **2012**, *24* (11), 1418–1423.
(29) Wang, Z.; Zong, S.; Yang, J.; Li, J.; Cui, Y. Dual-Mode Probe Based on Mesoporous Silica Coated Gold Nanorods for Targeting Cancer Cells. *Biosens. Bioelectron.* **2011**, *26* (6), 2883–2889.
(30) Gao, Z.; Burrows, N. D.; Valley, N. A.; Schatz, G. C.; Murphy, C. J.; Haynes, C. L. In Solution SERS Sensing Using Mesoporous Silica-Coated Gold Nanorods. *The Analyst* **2016**, *141* (17), 5088–5095.
(31) Gorelikov, I.; Matsuura, N. Single-Step Coating of Mesoporous Silica on Cetyltrimethyl Ammonium Bromide-Capped Nanoparticles. *Nano Lett.* **2008**, *8* (1), 369–373.
(32) Egger, S. M.; Hurley, K. R.; Datt, A.; Swindlehurst, G.; Haynes, C. L. Ultraporous Mesostructured Silica Nanoparticles. *Chem. Mater.* **2015**, *27* (9), 3193–3196.
(33) Taylor, A. B.; Michaux, P.; Mohsin, A. S. M.; Chon, J. W. M. Electron-Beam Lithography of Plasmonic Nanorod Arrays for Multilayered Optical Storage. *Opt. Express* **2014**, *22* (11), 13234.
(34) Yoon, S.; Lee, B.; Kim, C.; Lee, J. H. Controlled Heterogeneous Nucleation for Synthesis of Uniform Mesoporous Silica-Coated Gold Nanorods with Tailorable Rotational Diffusion and 1 Nm-Scale Size Tunability. *Cryst. Growth Des.* **2018**, *18* (8), 4731–4736.
(35) Rowe, L. R.; Chapman, B. S.; Tracy, J. B. Understanding and Controlling the Morphology of Silica Shells on Gold Nanorods. *Chem. Mater.* **2018**, *30* (18), 6249–6258.
(36) Wu, C.; Xu, Q.-H. Stable and Functionable Mesoporous Silica-Coated Gold Nanorods as Sensitive Localized Surface Plasmon Resonance (LSPR) Nanosensors. *Langmuir* **2009**, *25* (16), 9441–9446.
(37) Keller, E. L.; Kang, H.; Haynes, C. L.; Frontiera, R. R. Effect of Silica Supports on Plasmonic Heating of Molecular Adsorbates as Measured by Ultrafast Surface-

Enhanced Raman Thermometry. *ACS Appl. Mater. Interfaces* **2018**, *10* (47), 40577–40584.
(38) Keating, M.; Chen, Y.; Larmour, I. A.; Faulds, K.; Graham, D. Growth and Surface-Enhanced Raman Scattering of Ag Nanoparticle Assembly in Agarose Gel. *Meas. Sci. Technol.* **2012**, *23* (8), 084006.
(39) Liu, Y.-J.; Zhang, Z.-Y.; Dluhy, R. A.; Zhao, Y.-P. The SERS Response of Semiordered Ag Nanorod Arrays Fabricated by Template Oblique Angle Deposition. *J. Raman Spectrosc.* **2010**, *41* (10), 1112–1118.
(40) Gu, X.; Tian, S.; Zhou, Q.; Adkins, J.; Gu, Z.; Li, X.; Zheng, J. SERS Detection of Polycyclic Aromatic Hydrocarbons on a Bowl-Shaped Silver Cavity Substrate. *RSC Adv.* **2013**, *3* (48), 25989.
(41) Gu, H.-X.; Hu, K.; Li, D.-W.; Long, Y.-T. SERS Detection of Polycyclic Aromatic Hydrocarbons Using a Bare Gold Nanoparticles Coupled Film System. *The Analyst* **2016**, *141* (14), 4359–4365.
(42) Pastoriza-Santos, I.; Sánchez-Iglesias, A.; García de Abajo, F. J.; Liz-Marzán, L. M. Environmental Optical Sensitivity of Gold Nanodecahedra. *Adv. Funct. Mater.* **2007**, *17* (9), 1443–1450..
(43) Otto, A.; Bruckbauer, A.; Chen, Y. X. On the Chloride Activation in SERS and Single Molecule SERS. *J. Mol. Struct.* **2003**, *661–662*, 501–514.
(44) Liu, F.; Gu, H.; Yuan, X.; Lin, Y.; Dong, X. Chloride Ion-Dependent Surface-Enhanced Raman Scattering Study of Biotin on the Silver Surface. *J. Phys. Conf. Ser.* **2011**, *277*, 012025.
(45) Liu, Y.; Lu, Z.; Zhu, H.; Hasi, W. Characterization of a Chloride-Activated Surface Complex and Corresponding Enhancement Mechanism by SERS Saturation Effect. *J. Phys. Chem. C* **2017**, *121* (1), 950–957.
(46) Hao, J.; Meng, X. Recent Advances in SERS Detection of Perchlorate. *Front. Chem. Sci. Eng.* **2017**, *11* (3), 448–464.
(47) Mosier-Boss, P. A.; Lieberman, S. H. Detection of Anions by Normal Raman Spectroscopy and Surface-Enhanced Raman Spectroscopy of Cationic-Coated Substrates. *Appl. Spectrosc.* **2003**, *57* (9), 1129–1137.
(48) Kokaislova, A.; Parchansky, V.; Matejka, P. Surface-Enhanced Infrared Spectra of Nicotinic Acid and Pyridoxine on Copper Substrates: What Is the Effect of Temperature and Deposition Conditions? *J. Phys. Chem. C* **2015**, *119* (47), 26526–26539.
(49) Xu, X.-H. N.; Huang, S.; Brownlow, W.; Salaita, K.; Jeffers, R. B. Size and Temperature Dependence of Surface Plasmon Absorption of Gold Nanoparticles Induced by Tris(2,2'-Bipyridine)Ruthenium(II). *J. Phys. Chem. B* **2004**, *108* (40), 15543–15551.
(50) D'Errico, G.; Ortona, O.; Capuano, F.; Vitagliano, V. Diffusion Coefficients for the Binary System Glycerol + Water at 25 °C. A Velocity Correlation Study. *J. Chem. Eng. Data* **2004**, *49* (6), 1665–1670.
(51) Tripathi, A.; Emmons, E. D.; Christesen, S. D.; Fountain, A. W.; Guicheteau, J. A. Kinetics and Reaction Mechanisms of Thiophenol Adsorption on Gold Studied by Surface-Enhanced Raman Spectroscopy. *J. Phys. Chem. C* **2013**, *117* (44), 22834–22842.

(52) Zayak, A. T.; Choo, H.; Hu, Y. S.; Gargas, D. J.; Cabrini, S.; Bokor, J.; Schuck, P. J.; Neaton, J. B. Harnessing Chemical Raman Enhancement for Understanding Organic Adsorbate Binding on Metal Surfaces. *J. Phys. Chem. Lett.* **2012**, *3* (10), 1357–1362.
(53) Rausch, M. H.; Heller, A.; Fröba, A. P. Binary Diffusion Coefficients of Glycerol–Water Mixtures for Temperatures from 323 to 448 K by Dynamic Light Scattering. *J. Chem. Eng. Data* **2017**, *62* (12), 4364–4370.
(54) Kievsky, Y. Y.; Carey, B.; Naik, S.; Mangan, N.; ben-Avraham, D.; Sokolov, I. Dynamics of Molecular Diffusion of Rhodamine 6G in Silica Nanochannels. *J. Chem. Phys.* **2008**, *128* (15), 151102.
(55) Phan, H. T.; Haes, A. J. Impacts of PH and Intermolecular Interactions on Surface-Enhanced Raman Scattering Chemical Enhancements. *J. Phys. Chem. C* **2018**, *122* (26), 14846–14856.
(56) Yamaguchi, A.; Mekawy, M. M.; Chen, Y.; Suzuki, S.; Morita, K.; Teramae, N. Diffusion of Metal Complexes Inside of Silica−Surfactant Nanochannels within a Porous Alumina Membrane. *J. Phys. Chem. B* **2008**, *112* (7), 2024–2030.
(57) Son, H. Y.; Kim, K. R.; Lee, J. B.; Le Kim, T. H.; Jang, J.; Kim, S. J.; Yoon, M. S.; Kim, J. W.; Nam, Y. S. Bioinspired Synthesis of Mesoporous Gold-Silica Hybrid Microspheres as Recyclable Colloidal SERS Substrates. *Sci. Rep.* **2017**, *7* (1), 14728.
(58) Segur, J. B.; Oberstar, H. E. Viscosity of Glycerol and Its Aqueous Solutions. *Ind. Eng. Chem.* **1951**, *43* (9), 2117–2120.

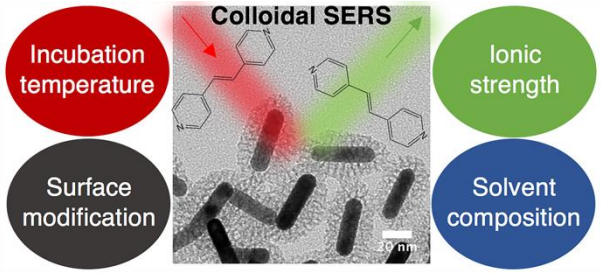

TOC Graphics